Electronic Supplementary Material (ESI) for Journal of Materials Chemistry A.

Effect of water frustration on water oxidation catalysis in the nanoconfined interlayers of layered manganese oxides birnessite and buserite.

Ravneet K. Bhullar, Michael J. Zdilla, Michael L. Klein, and Richard. C. Remsing

Supporting Information.

Contents

1. Computational Methods:
MODIFIED CHARGE FRUSTRATED XY MODEL

We write the Hamiltonian of the system as

$$H = H_{XY} + H_q + H_I \qquad (1)$$

corresponding to an XY model-like term, a Coulombic term, and a charge-XY interaction term. This is Hamiltonian is the same generic form as the charge frustrated XY model. We modify the Hamiltonian to account for out-of-plane degrees of freedom by introducing the additional spin variable z_i; $z_i = 0$ for an in-plane spin (solvent molecule), $z_i = +1$ for an out-of-plane spin point upward, and $z_i = -1$ for an out-of-plane spin pointing downward. The spin variables enter the modified charge frustrated XY model through the coupling constants $J_{XY}(z_i,z_j)$ and $J_I(z_i,z_j)$. Thus, the form of the Hamiltonians remains the same, but the coupling constants depend on the spin states of a central spin and its nearest-neighbors.

The Coulombic interaction term is unchanged by the additional degrees of freedom, and is given by

$$H_q = \frac{q^2}{2}\sum_{i \neq j} v(r_{ij}) s_i s_j t_i t_j \qquad (2)$$

where $v(r)$ is the Coulomb potential, which in two-dimensions is $-2\ln r$, s_i is the spin state of species *i* (1 for ions), and t_i is equal to 1 for cations, -1 for anions, and 0 for spins. The spin-ion interaction Hamiltonian is given by

$$H_I = -\sum_{\langle i,j \rangle} J_I(z_i,z_j) s_i t_i (1 - t_j) \cos \phi_{ij} \qquad (3)$$

where

$$J_I(z_i,z_j) = J_I(1 - t_i)\left[\left(1 - z_i^2\right) + z_i^2 b\right] + J_I(1 - t_j)\left[\left(1 - z_j^2\right) + z_j^2 b\right], \qquad (4)$$

the sum is over nearest-neighbor pairs, and $b < 1$ is a parameter that reduces the ion-spin interaction consistent with a dipole pointing out-of-plane. In this work, we set $b = 0.8$.

The additional spin degrees of freedom also alter the XY model-like piece of the Hamiltonian. This becomes

$$H_{XY} = -\sum_{\langle i,j \rangle} J_{XY}(z_i,z_j) \cos\left(\theta_i - \theta_j\right) \Theta(1 - t_i) \Theta(1 - t_j) \qquad (5)$$

where

$$J_{XY}(z_i,z_j) = J_{XY}\left[f_0^i f_0^j + f_+^i f_+^j + f_-^i f_-^j\right] + \frac{aJ_{XY}}{2}\left[f_0^i z_j^2 + f_0^j z_i^2 + f_+^i f_0^j + f_+^j f_0^i + f_-^i f_0^j + f_-^j f_0^i\right], \qquad (6)$$

$$f_0^i = \left(1 - z_i^2\right) \qquad (7)$$

$$f_+^i = \frac{z_i}{2}(1 + z_i) \qquad (8)$$

and

$$f_{-}^{i} = \frac{z_i}{2}(z_i - 1) \qquad (9)$$

The parameter *a* lowers the spin-spin interactions in a manner consistent with the weakening of dipole-dipole interactions between misaligned water dipoles, and we set *a* = 0.25 here.

To perform Monte Carlo simulations of the modified charge frustrated XY model, we carry out single-particle moves that change z_i, in addition to the single-particle spin moves and two-particle swap moves used in previous work (Ref. 6 of main text). Each move type is attempted with a probably of 1/3.

2. ICP-OES

Sample C	[Mn] µmol/L	[Na] µmol/L	[Ca] µmol/L
Ca Buserite	**222.009**	**6.684**	**153.952**
Ca Birnessite	**280.866**	**8.406**	**118.393**
Na Buserite	**101.358**	**13.373**	-
Na Birnessite	**258.817**	**101.559**	-
Dehydrated Birnessite	**258.817**	**101.559**	-

Table S1. Elemental content of the samples obtained from ICP Spectroscopy.

Determination of Mn Content. To determine total Mn content, 0.50 g of the samples were dissolved in hydroxylamine hydrochloride (0.5 M, 20 mL) and diluted to 250 mL. Mn content was then determined by analysis of an aliquot of the diluted solution by inductively coupled plasma optical emission spectrometry.

3. Turnover numbers.

Table S2. Turn over number (TON) and Turn over frequency (TOF) for the catalytic efficiency towards water oxidation

Sample	TON (mmol of O_2/mol of Mn)	TOF (mmol of O_2/mol of Mn . s)
Dehydrated Birnessite	198	0.598
Na Birnessite	114	0.268
Ca Birnessite	68	0.461
Ca Buserite	56	0.147
Na Buserite	11	0.0156

4. Elemental Analysis

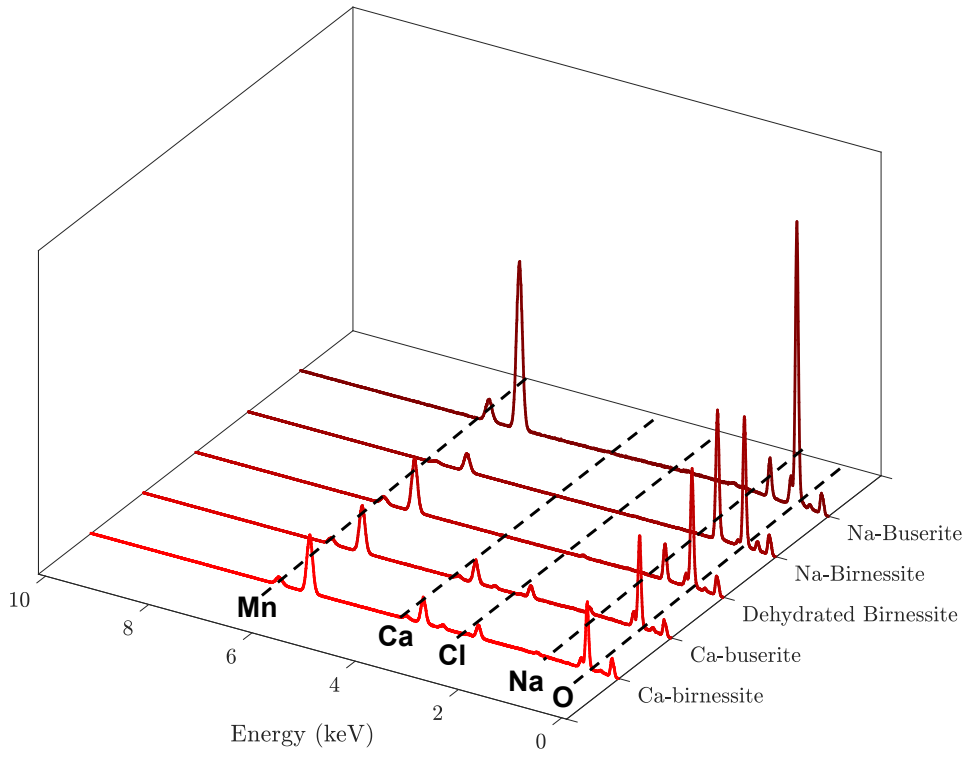

Figure S1. Elemental composition as measured by Energy dispersive spectroscopy, (EDS).

Table S3. Atomic composition measured by EDS.

Atomic composition (%)	Na-Birnessite	Na-Buserite	Ca-Birnessite	Ca-Buserite	Dehydrated Birnessite
Na	11.13	10.26	3.5	3.2	18.3
Mn	32.1	27	23.6	30.6	23.45
O	56.7	62.8	71	60.95	56.3
Ca	-	-	7.1	7.05	-
Cl	-	-	-	-	0.3

5. PXRD

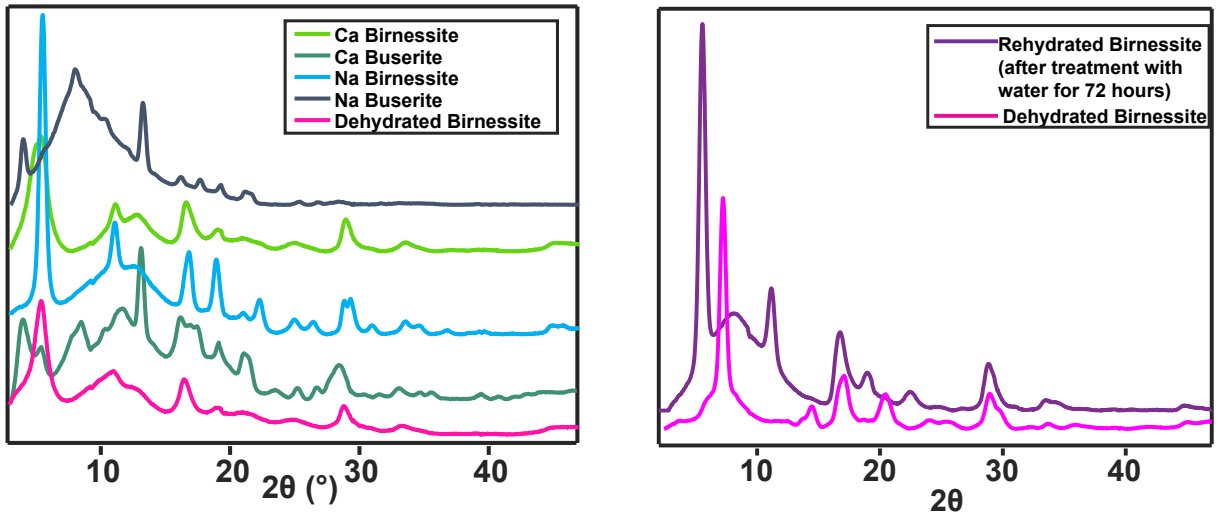

Figure S2. Left: PXRD pattern of birnessite, buserite and dehydrated birnessite recycled after catalysis. Right: PXRD of Dehydrated Birnessite after treatment with water for 72 hours.

Table S4. Indexed and refined unit cells.

Sample Name	Crystal Phase	Space Group (No.)	*a* (Å)	*b* (Å)	*c* (Å)	α (°)	β (°)	γ (°)
Na-Birnessite	Triclinic	*C*-1 (2)	5.1298	2.8445	7.2129	90.12	101.395	89.958
Na-Buserite	Triclinic	*C*-1(2)	5.1342	2.8469	10.200	90.31	101.559	89.944
Ca-Birnessite	Triclinic	*C*-1(2)	5.1349	2.8465	7.251	89.94	101.561	89.997
Ca-Buserite	Triclinic	*C*-1(2)	5.178	2.8509	10.200	89.45	103.18	89.91
Dehydrated-Birnessite	Triclinic	*P*-1(2)	2.9513	2.9547	5.651	78.72	101.79	122.33

6. TGA

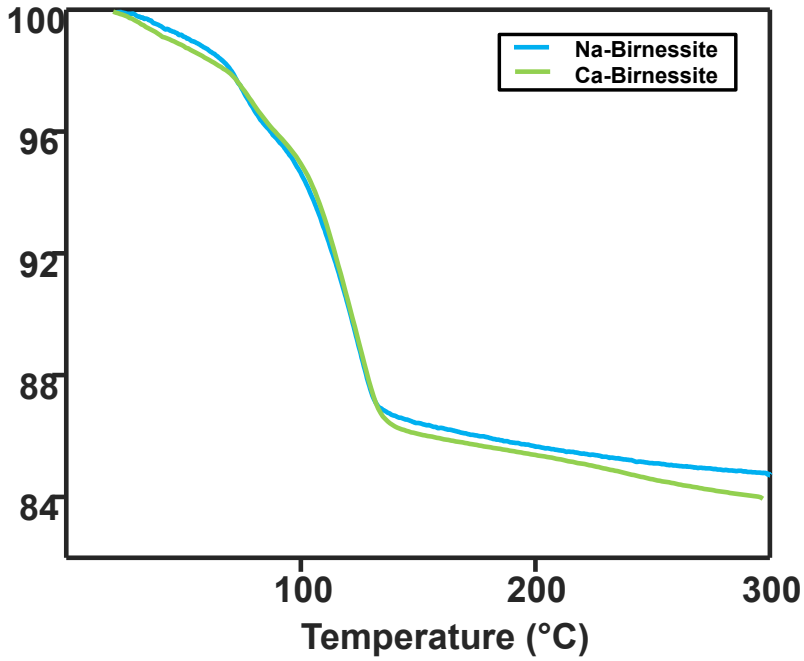

Figure S4. Thermogravimetric analysis (TGA) of Birnessite samples heated up to 300°C suggests 15.30% mass loss.

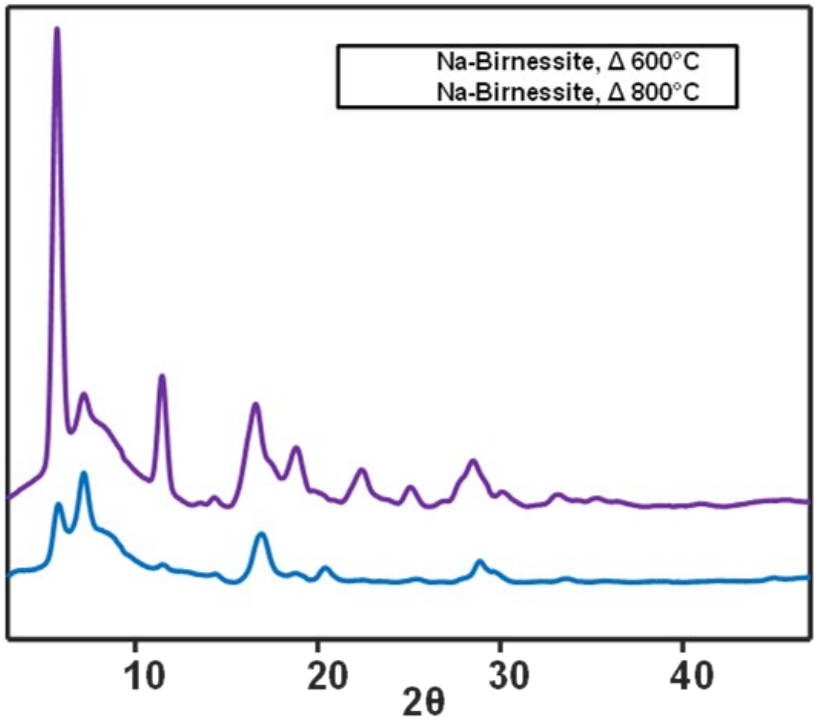

Figure S5. PXRD pattern of Na-Birnessite after Thermogravimetric analysis beyond 300°C indicating possible collapse of layered structure

7. Catalysis – extra figures.

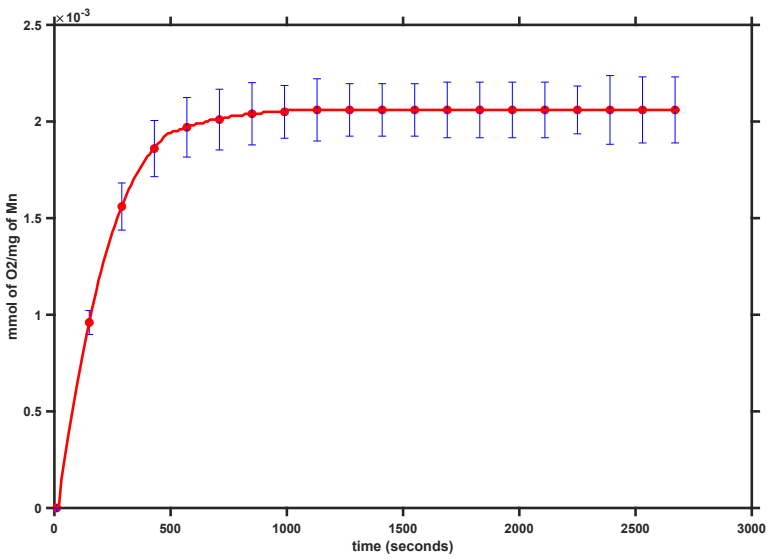

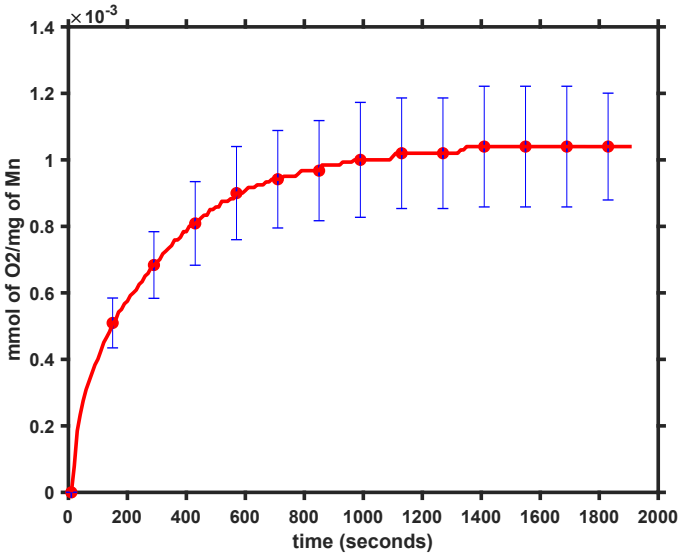

a. Na-Birnessite **b. Na-Buserite**

Figure S6(a,b). Standard deviation plot for the oxygen evolution reaction (OER). The tests were run in triplicate trials.

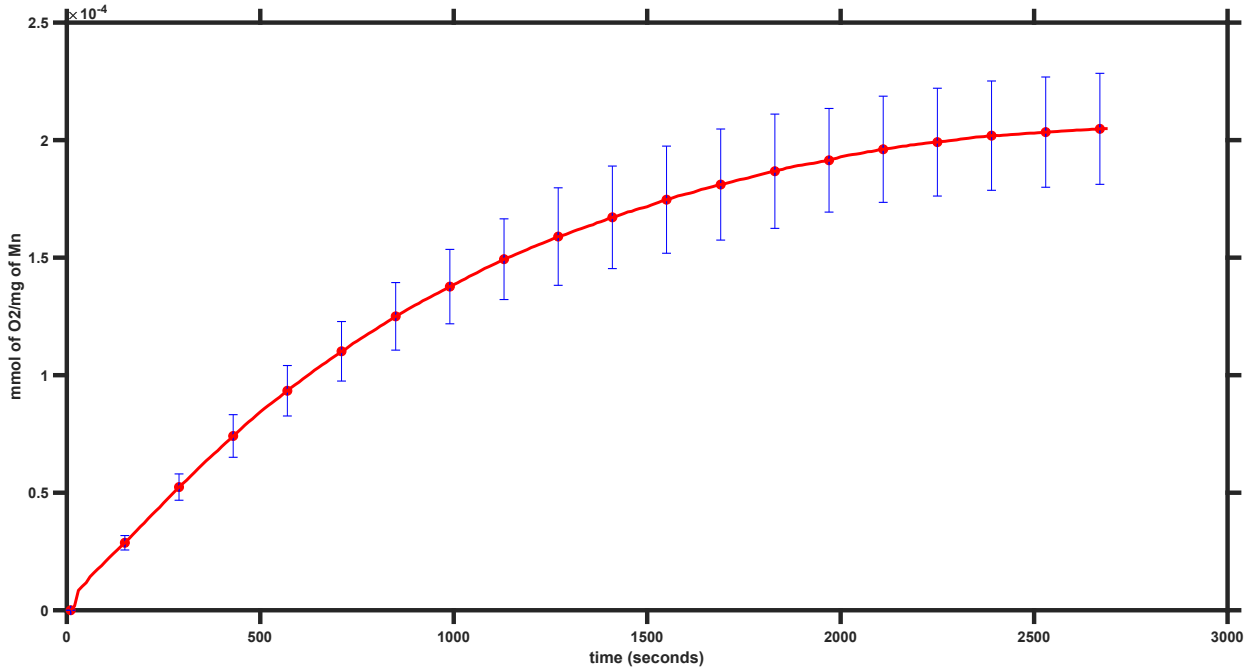

c. Ca-Birnessite

Figure S6(c). Standard deviation plot for the oxygen evolution reaction (OER). The tests were run in triplicate trials.

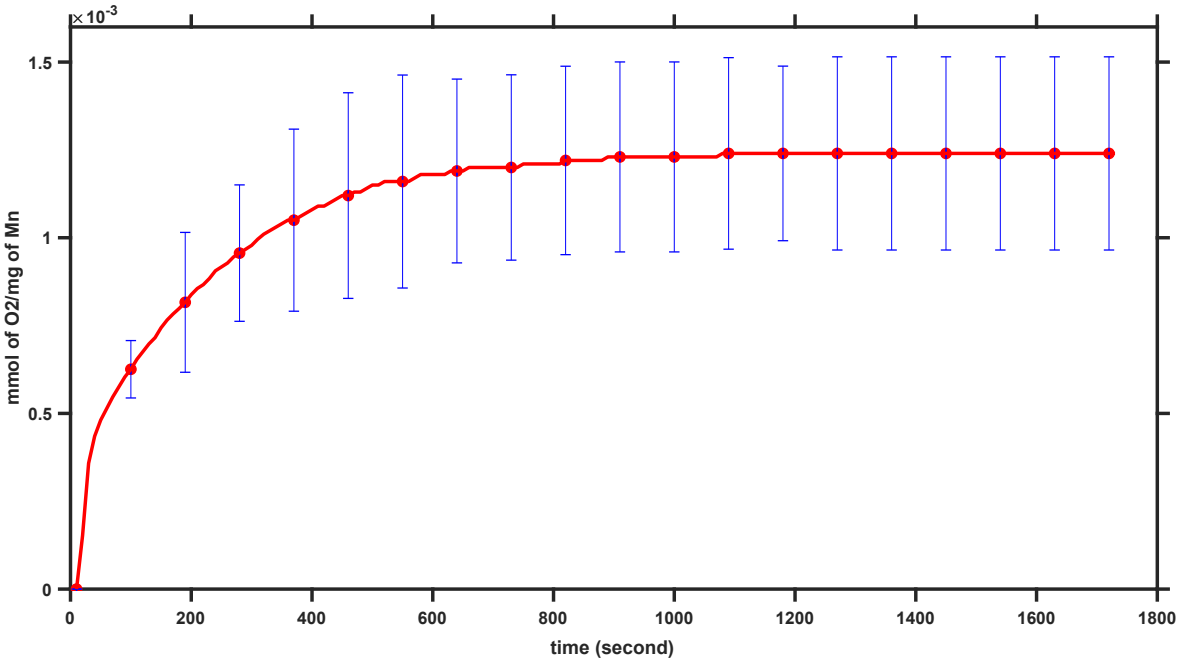

d. Ca-Buserite

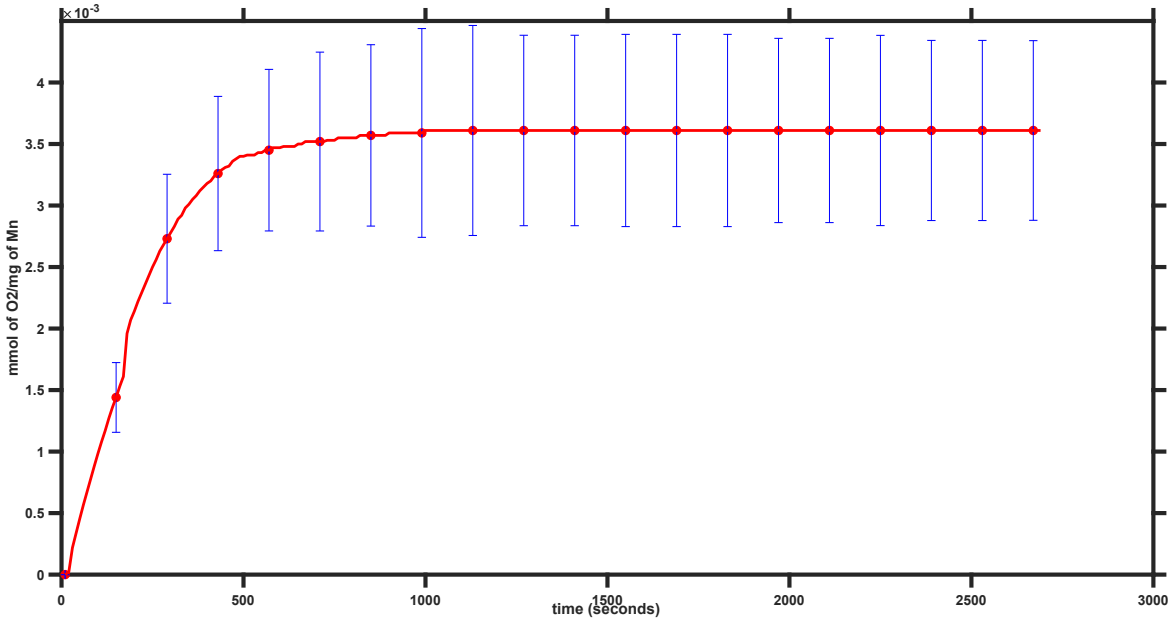

e. Dehydrated Birnessite

Figure S6(d, e). Standard deviation plot for the oxygen evolution reaction (OER). The tests were run in triplicate trials.

8. X-ray Photoelectron Spectroscopy

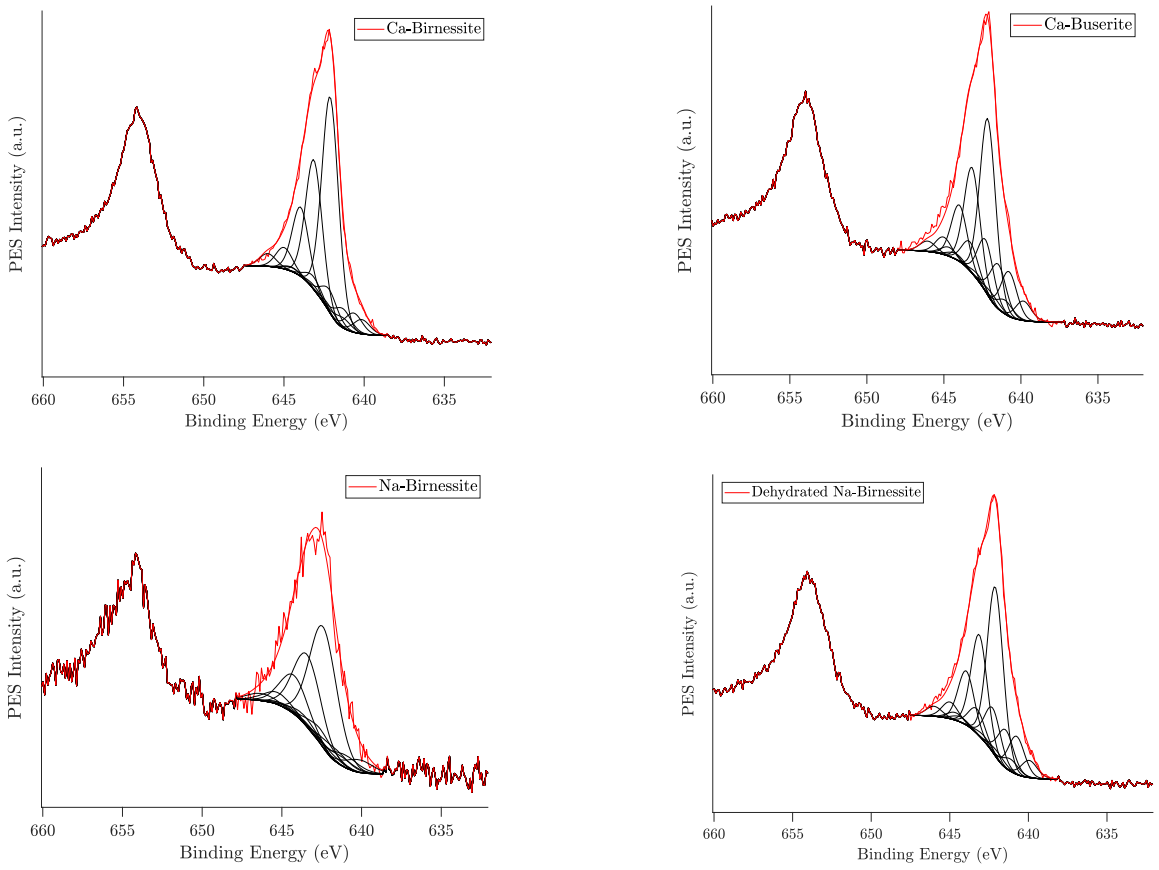

Figure S7. XPS spectra of Mn 2p. An analysis of Mn 2p3/2 indicates that the major species are Mn(IV) with small concentration of Mn(III) and Mn(II).

Table S5. Average oxidation state from fitting of XPS in Figure S7.

Sample Name	Average oxidation state
Dehydrated Na-Birnessite	3.55
Na-Birnessite	3.64
Ca-Birnessite	3.52
Ca-Buserite	3.72

9. Catalyst thickness and Electrochemical Surface Area

The thickness of the catalytic pellet on the electrode was measured using an optical microscope. The catalyst layer was viewed with the surface oriented parallel to the objective direction, and measured with an in-lens reticule. In all cases, the catalytic layer was approximately 150 μm in thickness.

The Electrochemical Surface Area (ECSA) was measured by comparison of the the electrochemical double layer capacitance (DLC) of our 7.1 mm^2 glassy carbon electrode to that of the catalyst samples. DLC response on the glassy carbon electrode was measured at several scan rates, and plots of the slope of positive and negative cathodic current gave statistically equivalent slopes, providing a normalized DLC response per mm^2. DLC measurements on birnessite and buserite samples were complicated by the existence of redox current at all potentials (no purely capacitative region), nevertheless, DLC response was measured as the half-distance between the cathodic and anodic currents centered around the flattest region of the cyclic voltammogram. ECSA was then determined using the following equation:

$$ECSA = 7.1\ mm^2\ (\frac{m_{cat}}{2m_{G.C.}})$$

…where 7.1 mm^2 is the area of the glassy carbon electrode, $m_{cat}/2$ is half the slope of the DLC response vs. scan rate plot for the catalyst (divided by two to calculate the anodic or cathodic current only), figure S9-S12, and $m_{G.C.}$ is the slope of the DLC cathodic (or anodic) response vs. scan rate plot for the glassy carbon electrode (Figure S8).

The resulting DLC response plots gave slopes with an intercept corresponding to redox current. While redox current may contribute to difference between cathodic and anodic currents, this technique thus represents an upper-bound measurement of ECSA.

Table S6. Electrochemical surface area (ECSA) and thickness of catalyst ink in electrochemical catalysis.

	ECSA (mm^2)	Thickness
Na-Birnessite	804.496	253.5
Ca-Birnessite	270.719	245.2
Ca-Busserite	416.295	241.3
Dehydrated Na-Birnessite	772.572	251.8

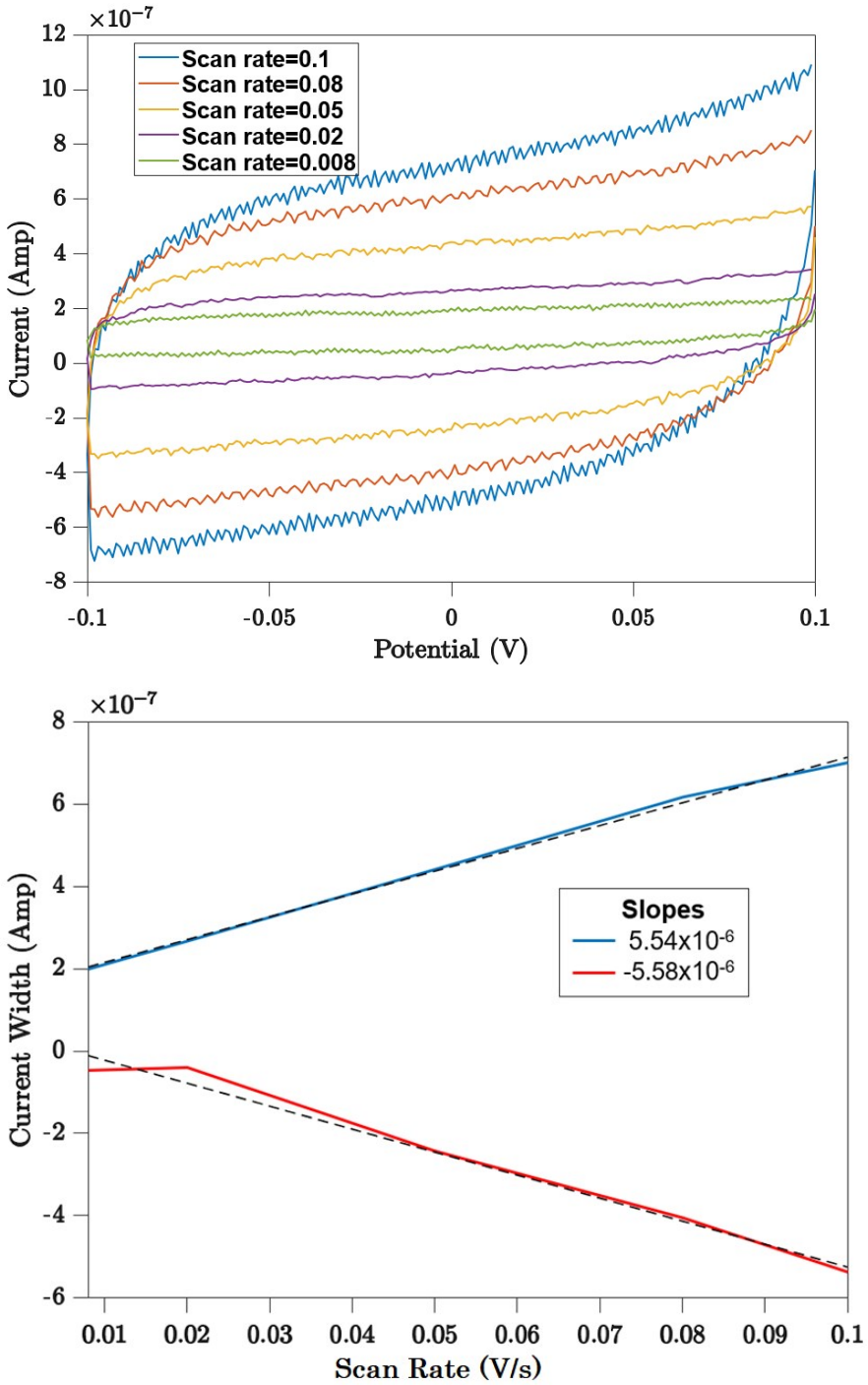

Figure S8. Top: Determination of DLC response of a 7.1 mm^2 glassy carbon electrode as a function of scan rate. Bottom: DLC current response (blue = positive and red = negative) vs. scan rate. Linear fit shown as dotted lines.

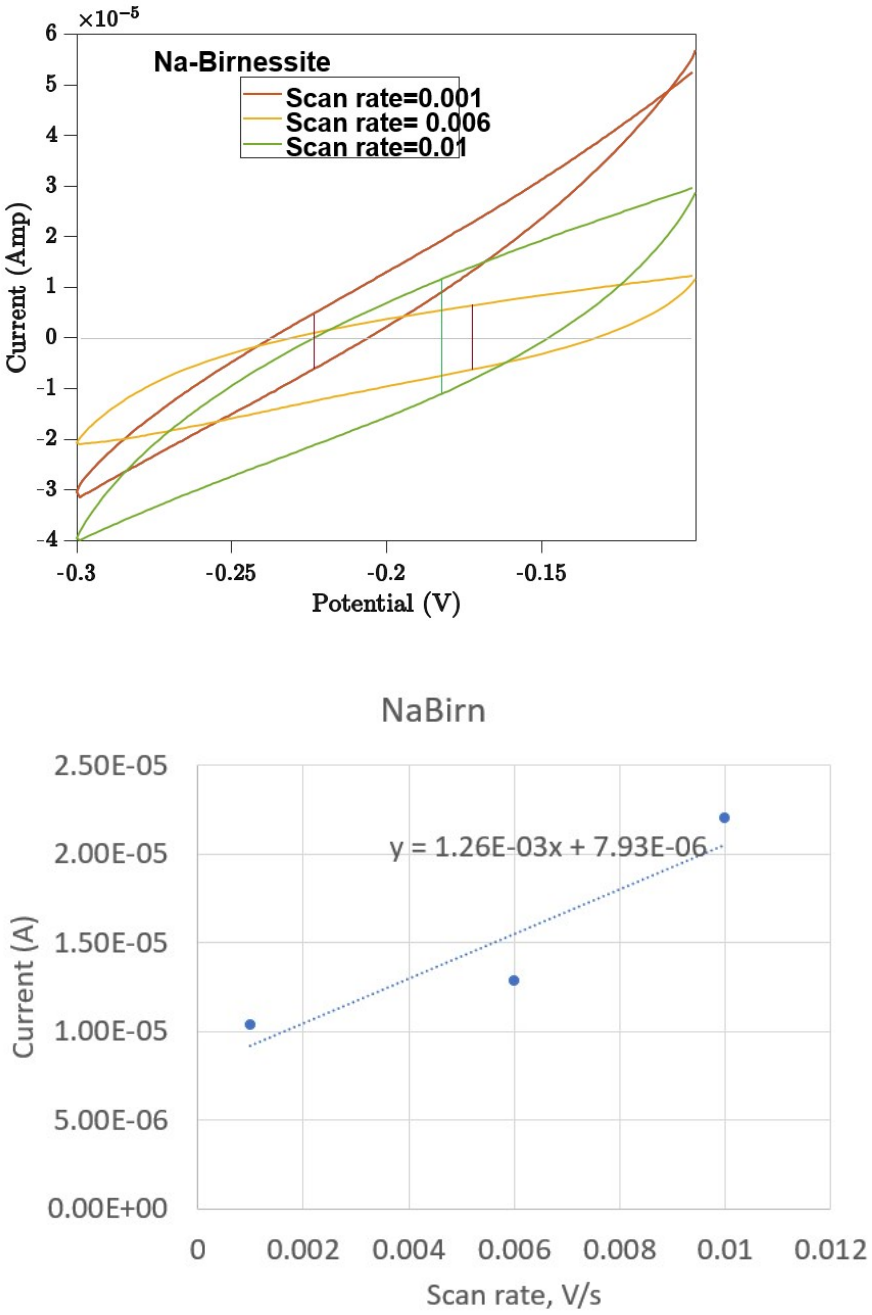

Figure S9. Top: Determination of DLC response of Na-birnessite sample as a function of scan rate. Bottom: DLC current response (I_{cath} - I_{anod}) vs. scan rate. Bottom: DLC vs. Scan rate, and linear fit shown as dotted line.

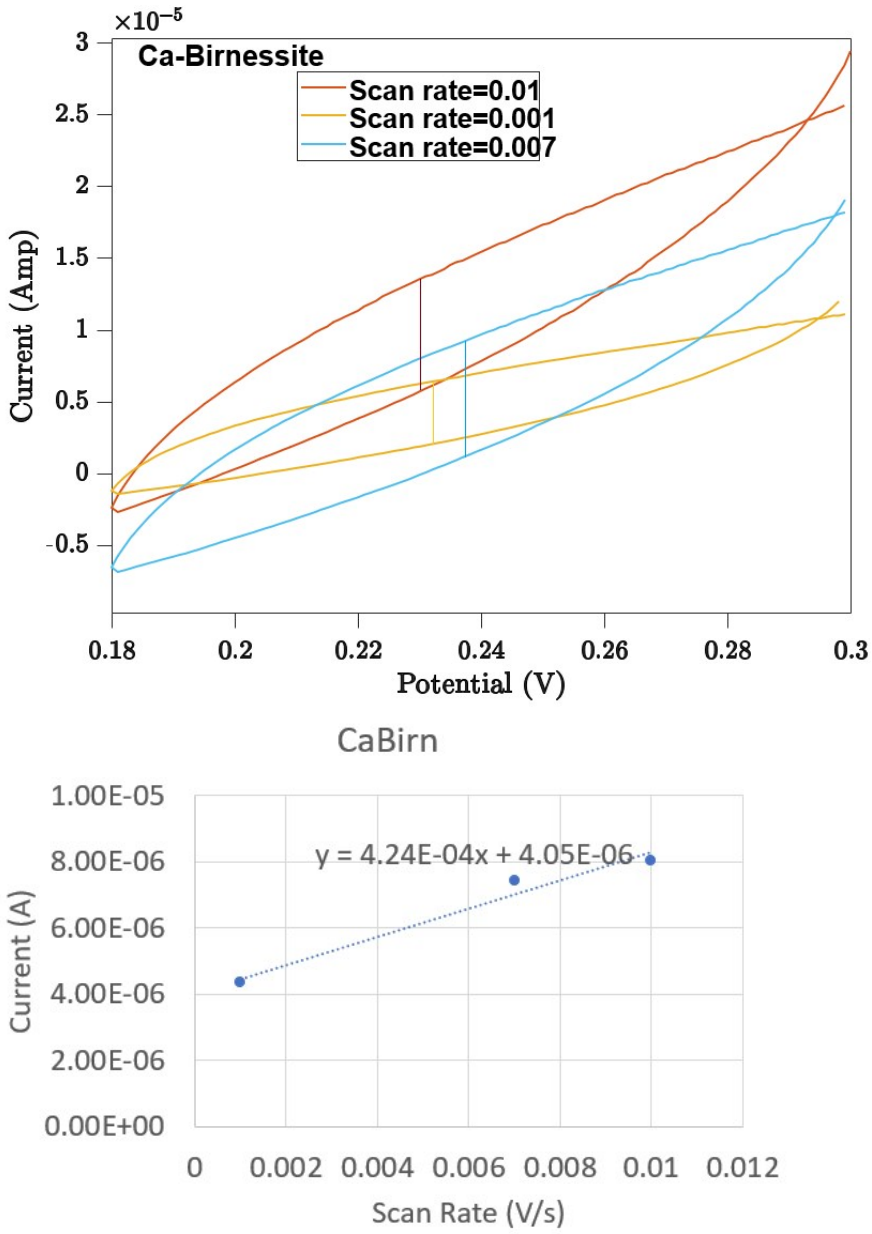

Figure S10. Top: Determination of DLC response of Ca-birnessite sample as a function of scan rate. Bottom: DLC current response (I_{cath} - I_{anod}) vs. scan rate. Bottom: DLC vs. Scan rate, and linear fit shown as dotted line.

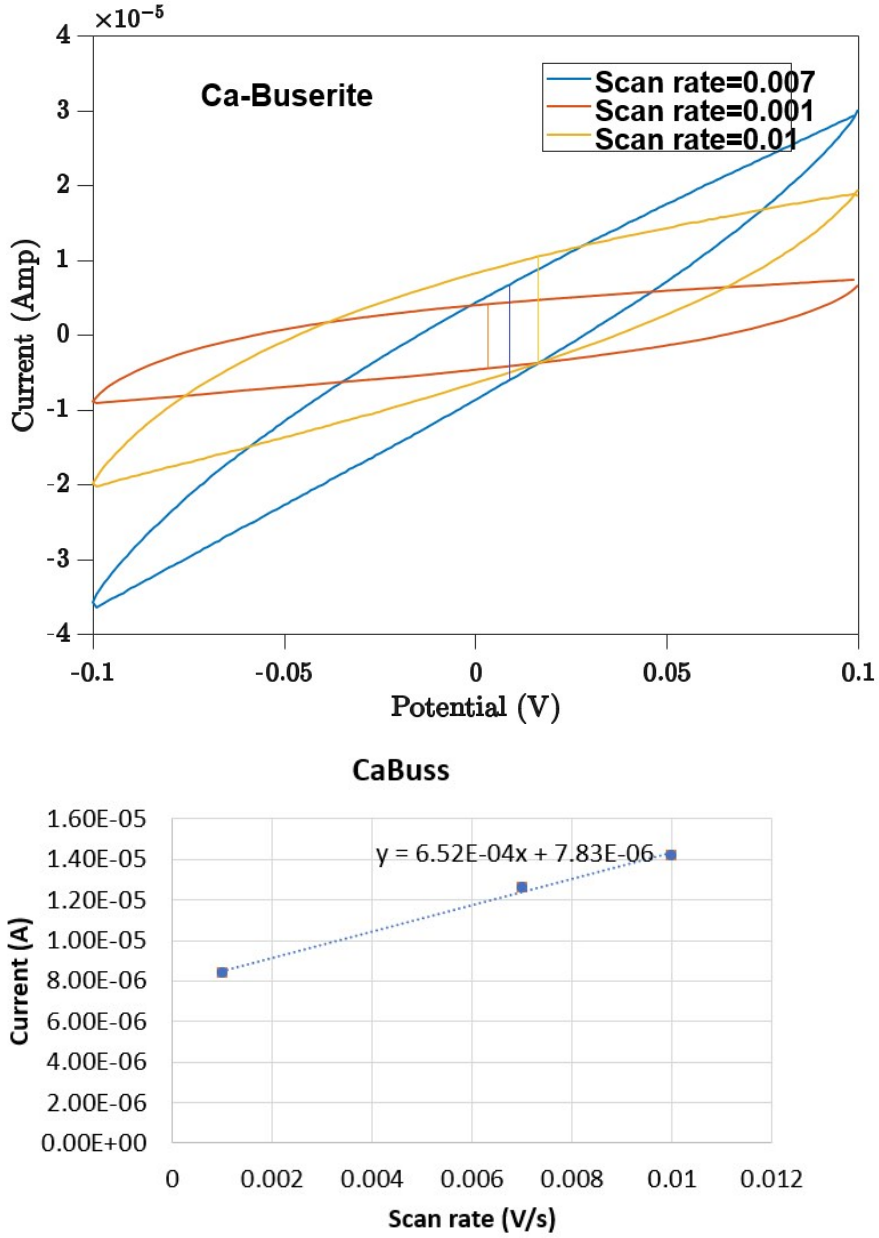

Figure S11. Top: Determination of DLC response of Ca-buserite sample as a function of scan rate. Bottom: DLC current response (I_{cath} - I_{anod}) vs. scan rate. Bottom: DLC vs. Scan rate, and linear fit shown as dotted line.

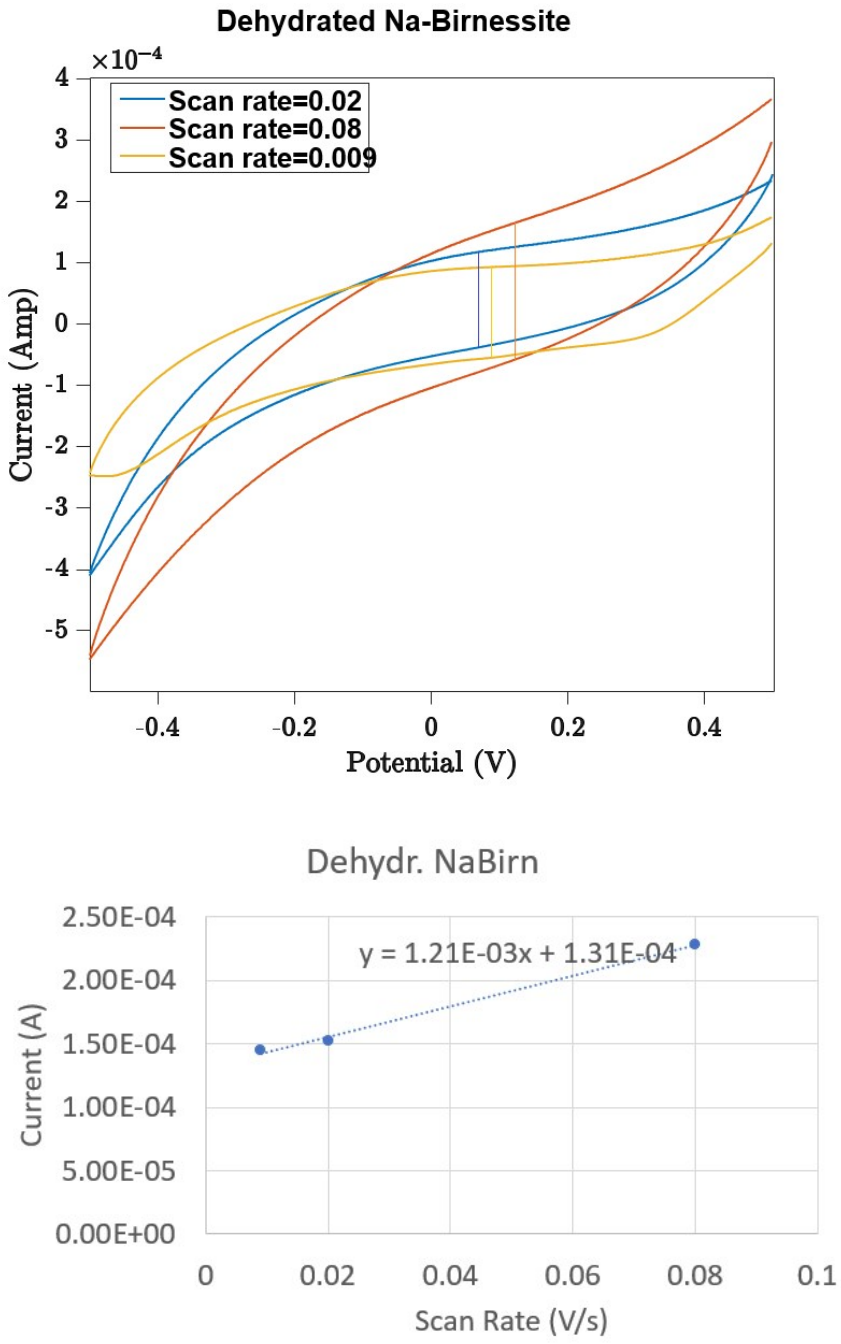

Figure S12. Top: Determination of DLC response of Ca-buserite sample as a function of scan rate. Bottom: DLC current response (I_{cath} - I_{anod}) vs. scan rate. Bottom: DLC vs. Scan rate, and linear fit shown as dotted line.